

# Fluid Dynamic Assessment of Three Polymeric Heart Valves Using Particle Image Velocimetry

HWA LIANG LEO,<sup>1,2</sup> LAKSHMI PRASAD DASI,<sup>1</sup> JOSIE CARBERRY,<sup>1</sup> HÉLÈNE A. SIMON,<sup>3</sup>  
and AJIT P. YOGANATHAN<sup>1</sup>

<sup>1</sup>Wallace H. Coulter School of Biomedical Engineering, Georgia Institute of Technology, Atlanta, Georgia; <sup>2</sup>Woodruff School of Mechanical Engineering, Georgia Institute of Technology, Atlanta, Georgia; and <sup>3</sup>School of Chemical and Biomolecular Engineering, Georgia Institute of Technology, Atlanta, Georgia

(Received 2 September 2005; accepted 23 March 2006; published online: 9 May 2006)

**Abstract**—Polymeric heart valves have the potential to reduce thrombogenic complications associated with current mechanical valves and overcome fatigue-related problems experienced by bio-prosthetic valves. In this paper we characterize the *in vitro* velocity and Reynolds Shear Stress (RSS) fields inside and downstream of three different prototype trileaflet polymeric heart valves. The fluid dynamic differences are then correlated with variations in valve design parameters. The three valves differ in leaflet thickness, ranging from 80 to 120  $\mu\text{m}$ , and commissural design, either closed, opened, or semi-opened. The valves were subjected to aortic flow conditions and the velocity measured using three-dimensional stereo Particle Image Velocimetry. The peak forward flow phase in the three valves was characterized by a strong central orifice jet of approximately 2 m/s with a flat profile along the trailing edge of the leaflets. Leakage jets, with principle RSS magnitudes exceeding 4,500  $\text{dyn}/\text{cm}^2$ , were observed in all valves with larger leaflet thicknesses and also corresponded to larger leakage volumes. Additional leakage jets were observed at the commissural region of valves with the open and the semi-open commissural designs. The results of the present study indicate that commissural design and leaflet thickness influence valve fluid dynamics and thus the thrombogenic potential of trileaflet polymeric valves.

**Keywords**—Heart valve, PIV, Particle Image Velocimetry, Thrombogenic, Polyurethanes, Coaptation, Washout, Trileaflet valve, Polymer.

## INTRODUCTION

Currently, mechanical prosthetic valves are the most widely implanted heart valve prostheses. Despite their superior hemodynamic properties and durability, they are prone to thromboembolic complications and thus patients are required to undergo lifelong anti-coagulation therapy.<sup>13,20</sup> Bioprosthetic valves, which are largely porcine in origin, are an alternative to the mechanical prostheses. However,

while tissue-based valves exhibit good hemodynamic performance, they are especially prone to calcification and tissue failure.

Polyurethane trileaflet polymeric heart valves constitute the latest development in prosthetic heart valve development.<sup>12</sup> Their design resembles that of the native human aortic valve and is therefore inherently appealing from a hemodynamic viewpoint. Polyurethane-based material has demonstrated excellent blood compatibility, hydrolytic stability, abrasion resistance, physical strength and flexure endurance.<sup>5,25,26</sup> Even though this particular valve design is still in a developmental stage, studies have shown it to possess excellent forward flow hemodynamic properties, equivalent to that of leading tissue heart valves, and the durability is expected to be comparable to that of mechanical heart valves.<sup>2,14</sup> Multiple *in vitro* studies have demonstrated that polymeric heart valves generate a centralized forward flow with a relatively flat velocity profile similar to that observed in bioprostheses and native heart valves.<sup>5,11,26</sup> The observed flow distribution is characterized by a central orifice jet flow with recirculation areas symmetrically located near the aortic wall downstream of the stent posts. However, polymeric heart valves were typically found to generate higher turbulent shear stresses than the tissue valves as a result of their more constricted flow orifices.<sup>5,25,26</sup> Chandran *et al.* investigated the effect of valve design on the flow dynamics distal to two trileaflet polyurethane valves and concluded that valves with the leaflets mounted outside the stents have a less obstructed flow orifice and thus better bulk flow than the ones with leaflets bound to the edge of the supporting stents.<sup>5</sup>

Recent animal trials involving polymeric valves have reported problems within six months of implantation associated with tearing of the leaflets and thrombus formation along the stent region of the valve.<sup>22</sup> Additionally, long-term *in vivo* evaluation has suggested that calcification could limit long-term function of polymeric valves. The leaflets and basal attachments, such as the

Address correspondence to Ajit P. Yoganathan, Wallace H. Coulter School of Biomedical Engineering, Georgia Institute of Technology, 313 Ferst Drive, UA Whitaker Building, Room 2119, Atlanta, Georgia 30332-0535 USA

commissural region, experience extrinsic calcification associated with surface microthrombus formation. The calcification appears to be independent of structural defects, suggesting that flow characteristics close to the polymeric valve structure contribute to the observed blood clots.

Previous studies on polymeric heart valves have taken two different approaches: (1) animal studies, investigating the biostability of various valve materials and the influence of valve designs on thrombus formation, and (2) hydrodynamic studies, investigating both the durability and downstream flow characteristics of various valve designs and materials. Currently, no detailed hemodynamics study has been conducted to investigate the flow inside a trileaflet polymeric heart valve prosthesis. Such a study would provide insight into the effects of design features, such as leaflet thickness and commissural designs, on blood damage potential. The aim of the current study is to examine in detail the flow structures inside and in the immediate vicinity of a trileaflet polymeric heart valve and to relate these flow structures to previously reported animal data on thrombus locations.

## METHODS

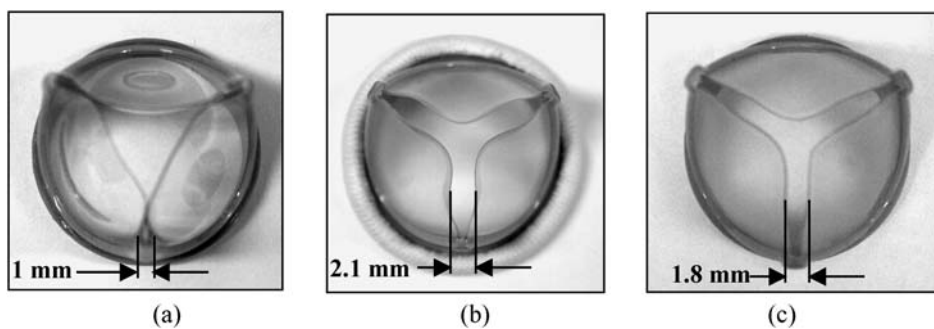
### *Studied Polymeric Heart Valves*

Figure 1 shows the three 23 mm trileaflet polymeric valves investigated in this study. The valves are prototype designs provided by AorTech Europe with leaflets manufactured from high silicone content polyurethane copolymer<sup>3</sup> (Elast-Eon<sup>TM</sup>) and valve frames and stents machined from poly-etheretherketone (PEEK). These polymeric valves were fabricated by dip-coating the PEEK frame with a thin layer of polyurethane to form the leaflets.<sup>18</sup> Therefore there is no variation in the material properties of the leaflets between the three valves. The free edge of each leaflet was fabricated such that it is equal to the valvular orifice diameter,  $D$  ( $= 23$  mm), and therefore total free-edge length equals 69 mm. Each of the three valves has a height of 14.3 mm and an effective orifice diameter of

23 mm. The variation in the commissural region between the three valves is indicated in the figure. Figure 2 shows the relevant terminology describing the different regions of interest on and in the vicinity of the valve. The commissural region is defined as the region where the leaflets meet near a stent post. A closed commissural design is characterized by two adjacent leaflets in the stent post region. As these leaflets wrap around the stent post, a small channel (termed gap channel) forms along the stent inflow region, where the stent inflow region is defined as the region along the stent inside the polymeric valve. In an open commissural design the adjacent leaflets do not come together near the stent but are well-separated. The coaptation region denotes the location where the three leaflets meet while the high central region of the valve is located at the upper portion of the each leaflet near its free edge. As shown in Fig. 1, Prototype A valve has a closed commissure design with a mean leaflet thickness of  $80 \mu\text{m}$  and a gap channel diameter of approximately 1.0 mm. Prototype B valve has an open commissure design with a mean leaflet thickness of  $120 \mu\text{m}$  while prototype C has a semi-open commissure and a mean leaflet thickness of  $120 \mu\text{m}$ . Both prototypes B and C do not form a gap channel at the commissural region during the unstressed state; the distance between adjacent leaflets near the commissural region for prototypes B and C is 2.1 mm and 1.8 mm, respectively. The three valves are shown in their free, or unstressed, state. The flow fields in the vicinity of these three valves are studied to determine the effect of leaflet thickness and commissural design on the fluid dynamic performance.

### *Physiological Flow Loop*

The valves were placed in a transparent polycarbonate test chamber to enable three-dimensional stereo Particle Image Velocimetry (3D PIV) flow measurements. The valves were mounted in the aortic position of the Georgia Tech left heart simulator<sup>16</sup> (shown in Fig. 3) and subjected to physiological aortic flow conditions. The flow loop, driven by a pulse generator, consisted of tubing, a mechanical valve in



**FIGURE 1.** Top view of the 23 mm Aortech polymeric heart valves in their unstressed state: (a) prototype A, closed commissure with  $80 \mu\text{m}$  leaflet thickness; (b) prototype B, opened commissure with  $120 \mu\text{m}$  leaflet thickness; (c) prototype C, semi-opened commissure with  $120 \mu\text{m}$  leaflet thickness.

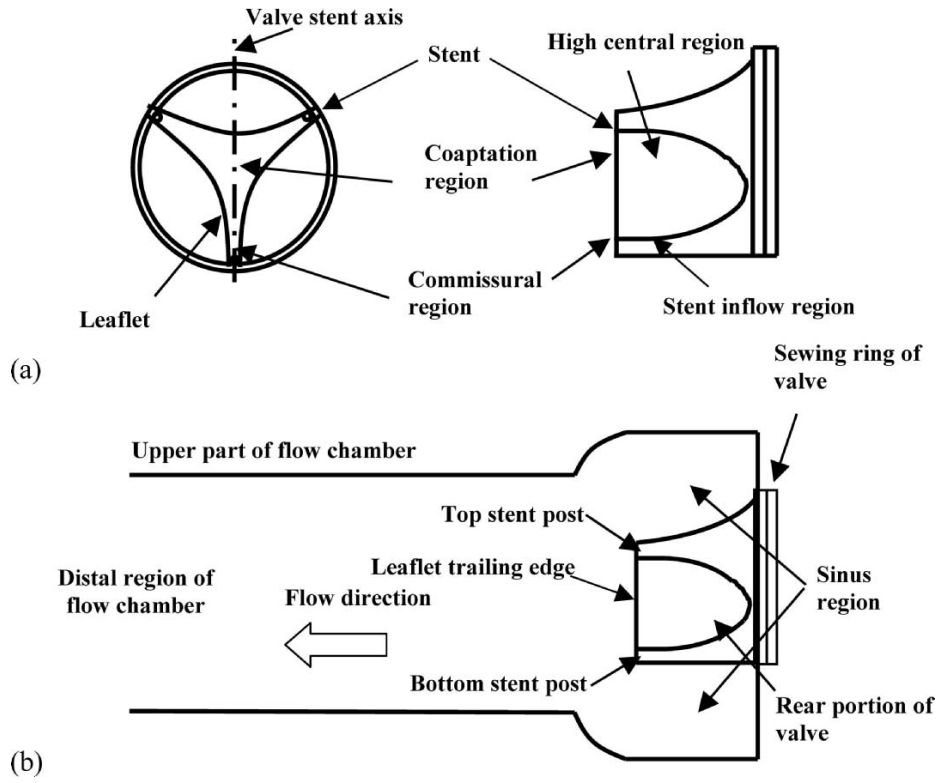


FIGURE 2. Pertinent terminology for the three 23 mm Aortech trileaflet polymeric heart valves: (a) on the valve superstructure; (b) defining the locations downstream of the valve inside the flow chamber.

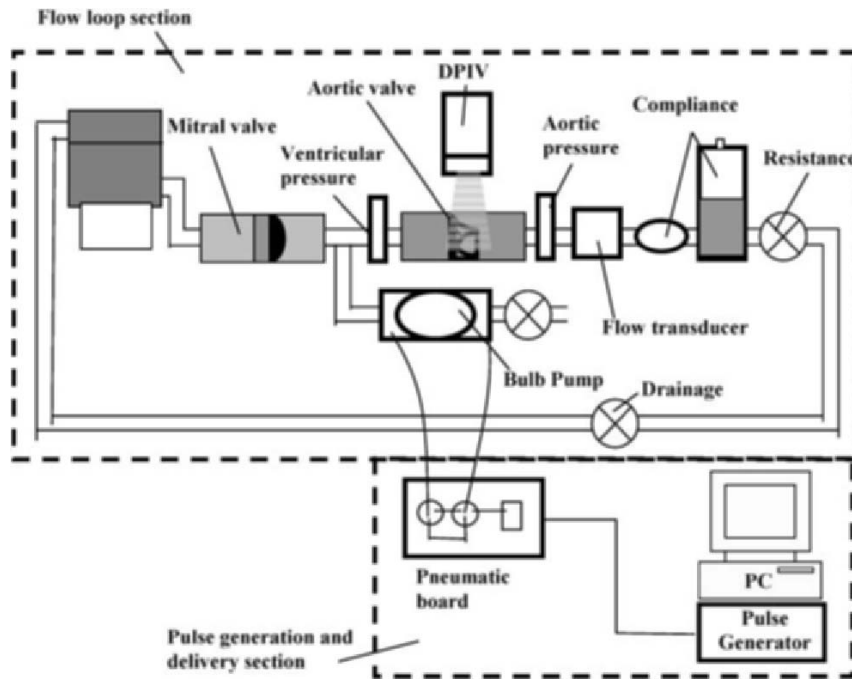


FIGURE 3. Pulsatile loop setup for the aortic valve experiments.

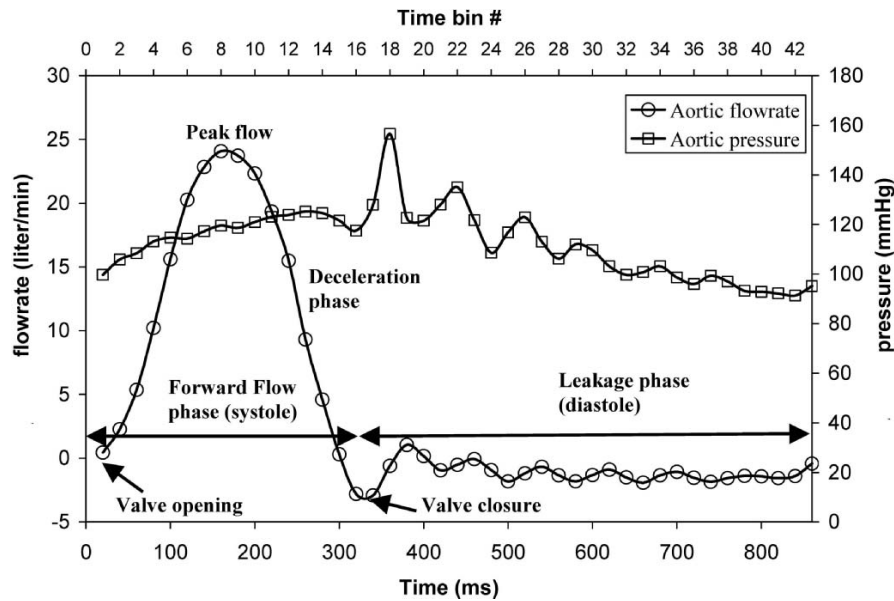


FIGURE 4 Aortic valve flow rate and pressure waveforms.

the mitral position, a flow transducer, ventricular and aortic pressure transducers, a bulb pump, compliance, and resistance.<sup>16</sup> Variation of the compliance and resistance sections of the loop allowed additional control in order to produce physiological flow and pressure waveforms. The heart rate was set at 70 beats/min with a cardiac output of 5.0 L/min, a peak systolic flow rate of 25.0 L/min, a mean aortic pressure of 90–100 mmHg and a systolic flow phase duration of approximately 35% of the cardiac cycle time. A detailed description of the flow loop can be found in literature.<sup>16</sup> Figure 4 shows the resulting physiological flow and pressure waveforms.

The working fluid was a solution of 79% saturated aqueous sodium iodide, 20% glycerin, and 1% water by volume. This blood analog fluid had a kinematic viscosity of 3.5 cSt, to match that of blood at high shear rates, and its refractive index was adjusted to match that of the valve-mounting chamber (1.49), thereby minimizing optical distortion.

#### Particle Image Velocimetry (PIV)

A 3D PIV system was used to acquire planar three-dimensional velocity measurements inside and in the immediate vicinity of the polymeric trileaflet heart valves. The system consisted of two Nd:YAG lasers (Model MiniLaser-I, New Wave Research, CA) with an energy of 17 mJ per pulse and a maximum repetition rate of 15 Hz. An articulated laser arm (Model 610015, TSI, MN) was used to direct the laser (laser sheet thickness  $\sim 1.0$  mm thickness) to the area of investigation. Fluorescent polymeric particles based on melamine resin of diameter 1–20  $\mu\text{m}$  (FPP-RhB-10, Dantec Dynamics, Denmark) were used in combination with an orange filter (Quantaray, Wolf Camera) to eliminate

reflections from the model surface at the laser excitation wavelength (532 nm). The images were recorded using two cross-correlation CCD cameras (Model 1101MPRO, LaVision, Germany) of  $1600 \times 1200$  pixel resolution. These cameras are capable of capturing PIV image pairs at a maximum rate of 12 Hz. Each camera was fitted with 60 mm AF lenses (1:2.8D, Nikon) and a Scheimpflug mount (Model 1108196, LaVision, Germany). Stereo images were generated with an angle of  $25^\circ$  between the cameras. The 3D PIV measurement plane had a field of view of approximately  $56 \text{ mm} \times 42 \text{ mm}$ . The final interrogation window was  $16 \times 16$  pixels yielding a spatial resolution of  $0.4 \text{ mm} \times 0.4 \text{ mm}$ . By triggering the PIV system from the pulse generator driving the bulb pump, phase-locked measurements were acquired, over 43 equally distributed time bins along the 860 ms cardiac cycle. An ensemble of 250 pair images was acquired by phase locking to each of the 43 time points corresponding to a sampling rate of 1.167 Hz (70 beats per min). The laser pulse separation was adjusted for each of the 43 phases of the cardiac cycle via a trial and error approach and ranged from  $75 \mu\text{s}$  during the systolic phase to  $500 \mu\text{s}$  during the diastolic phase to accurately capture prominent flow structures. The pulse separation rates were chosen such that the maximum pixel displacement of the PIV particles corresponded to the dynamic range allowable for a  $64 \times 64$  interrogation window (corresponding to the first PIV interrogation pass before subsequent passes of smaller interrogation windows).

#### Calibration

Correction for off-axis viewing was performed by taking preliminary images of the flow, and then, without shifting

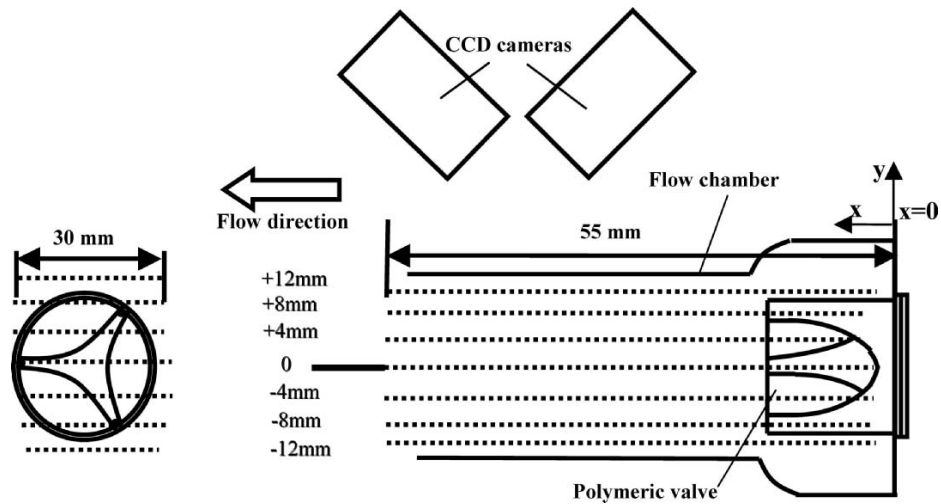


**FIGURE 5.** Measurement planes (*dotted lines*) corresponding to the 3D PIV experiments. All downstream measurements were made with reference from the valve sewing ring, which is marked  $x=0$ .

the distance between the cameras and the laser sheet or the angle between the cameras, the test section was replaced with the calibration target so that it was aligned with the laser sheet. The calibration target was a two-dimensional array of dots at a known spacing placed onto the back of a transparent  $150 \times 95 \times 19 \text{ mm}^3$  acrylic block. Images of the target plate were captured, and skewing of the images was taken into account in Davis 7.0 software (LaVision, Germany). This information was stored as the calibration set file and was used to process the preliminary flow data to output a final calibration set file. The final correction file was used for subsequent 3D PIV data processing.

#### *Measurement Locations*

Velocity measurements were acquired along seven measurement planes parallel to the valve stent axis, as shown in Fig. 5 with the center of the valve chosen as the reference plane. The orientation for the valve stent axis is illustrated in Fig. 2(a). The distance between the laser sheet and the cameras was fixed throughout the measurements. The translation between measurement planes was achieved by moving the valve chamber, which was marked with an equally spaced grid on either end of the chamber assembly. The locations of all downstream measurements were referenced from the valve sewing ring, marked  $x=0$  on Fig. 5.

## **RESULTS**

All of the results presented are derived from ensemble-averaged fields. The flow characteristics of prototype A will be discussed first, followed by those of prototypes B and C. Flow characteristics of greatest interest were observed in the center and  $+8 \text{ mm}$  symmetry planes; therefore the

following result section is based primarily on these measurement planes.

#### *Prototype A Center Plane*

##### *Systole*

During the acceleration phase, a central orifice jet of  $1.0 \text{ m/s}$  was observed issuing from the orifice of the valve, forming a vortex ring along the edge of the jet. The central orifice flow reached a maximum velocity magnitude of  $2.4 \text{ m/s}$  at peak systole in the vena contracta region, approximately  $20 \text{ mm}$  downstream of the valve sewing ring (Fig. 6). A maximum velocity of  $2.0 \text{ m/s}$  was measured at the trailing edge of the leaflet inside the valve at peak systole, with low velocity flow of  $0.5 \text{ m/s}$  along the stent inflow region of the valve throughout systole. The central orifice jet had a diameter of approximately  $13 \text{ mm}$  at the trailing edge of the leaflet. Figure 6 shows that the flat velocity profile of the central orifice jet exiting from the valve orifice becomes parabolic approximately  $45 \text{ mm}$  downstream from the valve sewing ring. Flow separation was observed at the trailing edge of the leaflet. Two reattachment points occurred downstream from the valve sewing ring: one in the upper part of the flow chamber occurred beyond the measurement plane, while another in the lower part of the flow chamber was  $55 \text{ mm}$  downstream of the valve sewing ring. A peak velocity of  $0.6 \text{ m/s}$  was seen inside the recirculation zone. Flow in the sinus region was generally less than  $0.02 \text{ m/s}$  with transient vortex structures appearing briefly during the acceleration and deceleration phases. Figure 7 displays the iso-surface of the velocity magnitude downstream of valve A at peak systole. The iso-surface was characterized by a three lobe profile, which became clearly evident  $55 \text{ mm}$  downstream of the valve sewing ring. Each lobe



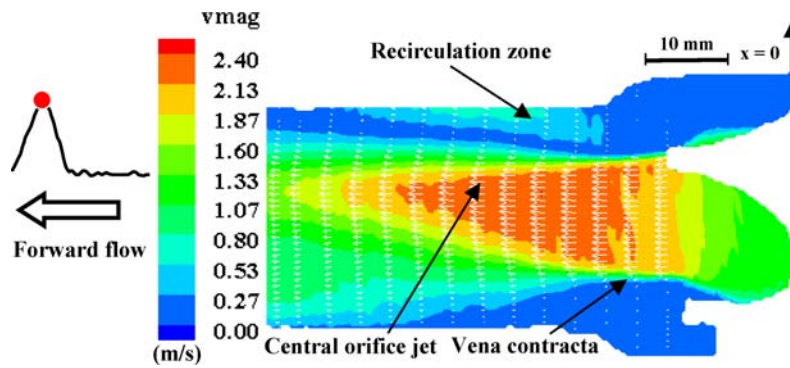


FIGURE 6. Phase-averaged velocity measurement at the center plane of prototype A at peak systole. Central orifice jet of magnitude 2.3 m/s was observed issuing from the valve orifice with flow separation occurring at the trailing edge of the leaflet.

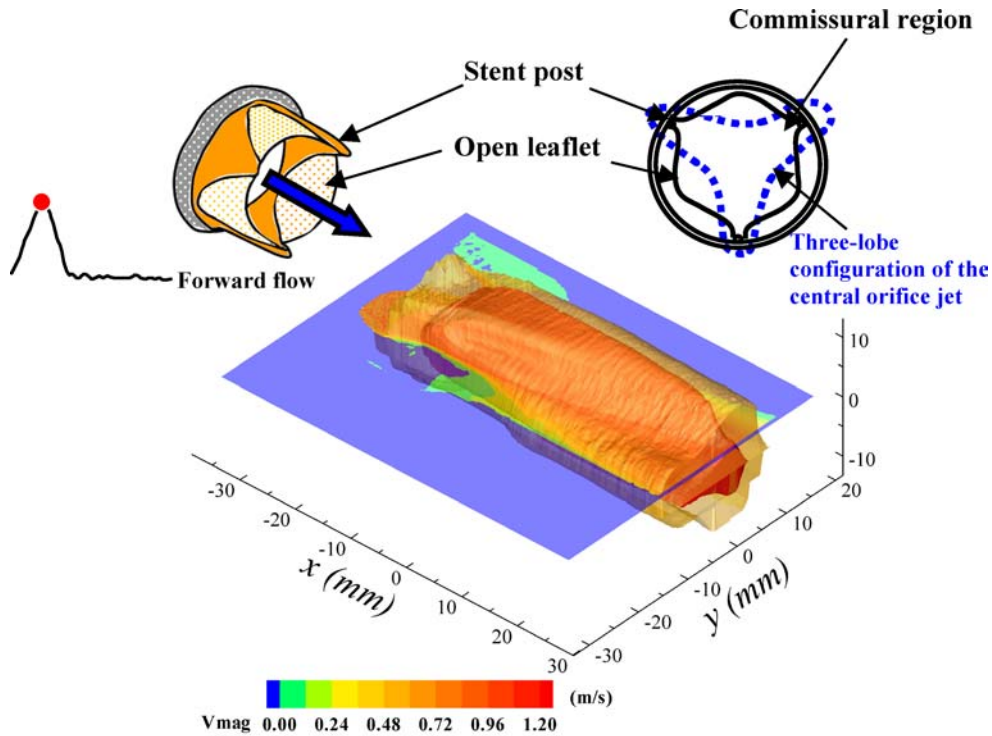


FIGURE 7. Iso-surface of velocity magnitude downstream of prototype A at peak systole. Top right of figure shows that each lobe coincided with the commissural region of the valve.

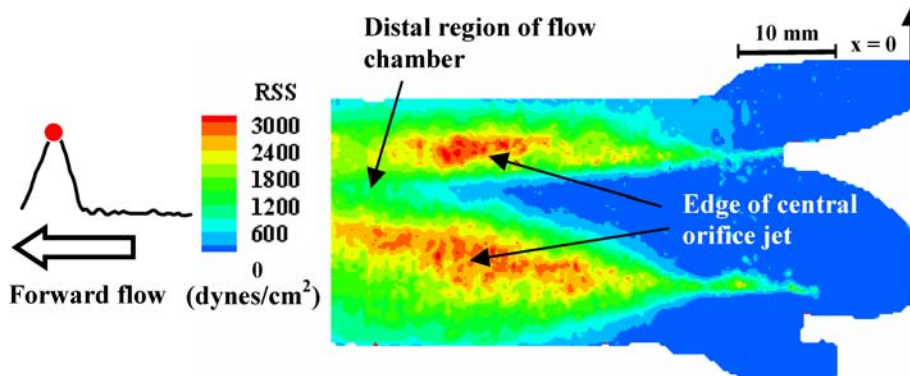
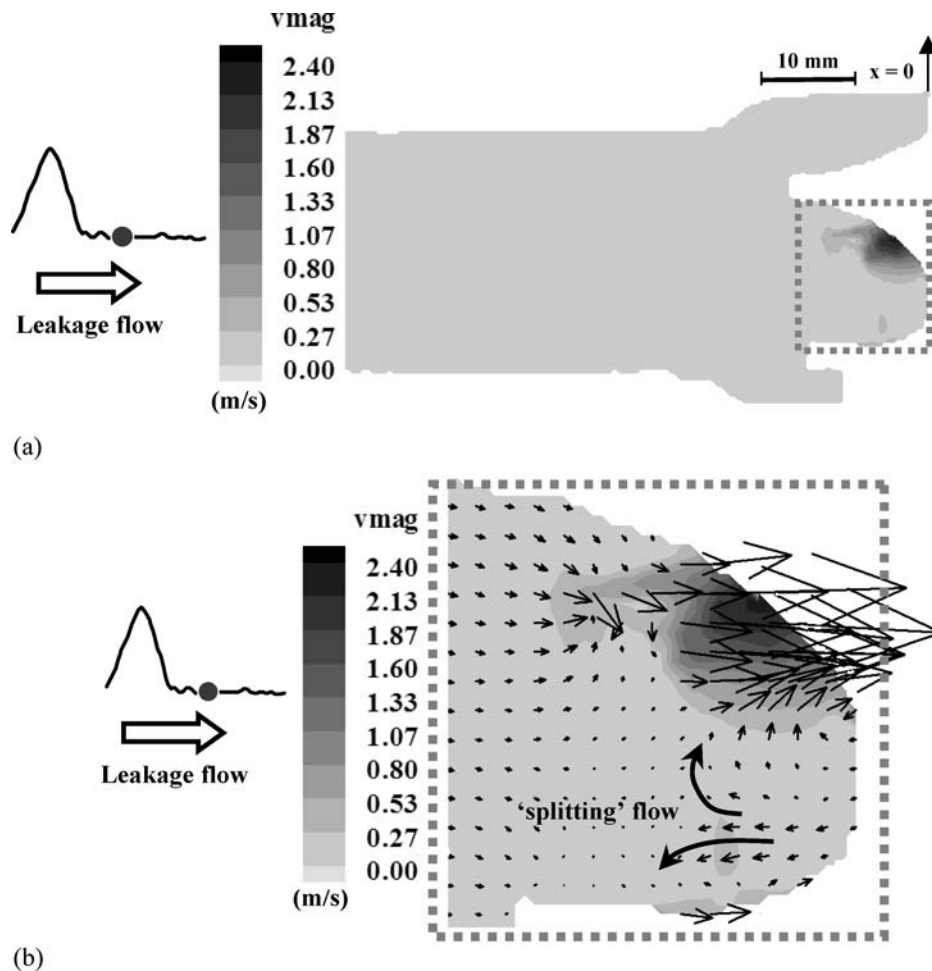


FIGURE 8. Reynolds shear stress (RSS) contour plot at the center plane of prototype A at peak systole. High RSS values coincided with regions of high velocity gradient typically observed at the edge of the central orifice jet and at the distal part of the flow chamber.



**FIGURE 9.** Phase-averaged velocity measurement at the center plane of prototype A during mid-diastole. (a) downstream of the valve (b) inside the valve (the flow field inside the enlarged *dotted box* of Fig. 9(a)).

coincided with a region of high velocity flow issuing from the commissural region.

During the deceleration phase, the velocity in the central orifice jet decreased from 2.4 to 1.1 m/s, while the velocity in the recirculation zone observed in the upper part of flow chamber was reduced from 0.6 to 0.4 m/s.

Figure 8 shows the Reynolds shear stress (RSS) distribution for prototype A at peak systole. RSS levels of more than 3,000 dyn/cm<sup>2</sup> were observed in three regions: in the shear layer region between the central orifice jet and the surrounding fluid, at the trailing edge of the leaflet, and in the region of turbulence 55 mm downstream of the valve sewing ring. The RSS levels outside these regions were typically less than 3,000 dyn/cm<sup>2</sup>.

#### Diastole

The velocities downstream of the trailing edge of the leaflet during diastole were typically less than 0.02 m/s,

except for the flow inside a recirculation zone along the wall of the valve chamber during early diastole, which generated velocity magnitudes up to 0.4 m/s. The velocity inside this recirculation zone decreased to less than 0.02 m/s during late diastole. Inside the valve a leakage jet with a velocity of 1.63 m/s was observed at the high central region during mid-diastole (Fig. 9a). Leakage flow was also seen near the commissural region along the stent post during early diastole. Flow inside the valve was split and directed towards either the stent post or the high central region [Fig. 9(b)]. This splitting flow phenomenon persisted throughout diastole, becoming more noticeable when the leakage jets in the high central region and commissural regions appeared. Elevated RSS levels of 5,000 dyn/cm<sup>2</sup> were observed in the leakage jet at the high central region of the valve. In contrast, the RSS levels in the flow field downstream of the leaflet trailing edge were typically less than 100 dyn/cm<sup>2</sup>.

*Prototype A + 8 mm Offset Plane**Systole*

During the acceleration phase, the forward flow jet at the + 8 mm offset plane emanated from the commissural region of the valve, generating maximum velocity magnitudes of up to 0.8 m/s in the forward flow jet, approximately 25 mm downstream from the valve sewing ring. At peak systole (Fig. 10), the forward flow jet reached a maximum velocity of 2.1 m/s, reducing to approximately 1.6 m/s 55 mm downstream of the valve sewing ring. Flow separation occurred at the trailing edge of the leaflet and flow reattachment was observed approximately 27 mm and 50 mm downstream of the valve sewing ring in the upper and lower parts of the flow chamber, respectively. Inside the valve, the flow near the trailing edge of the leaflet reached a maximum velocity of 2.0 m/s at peak systole, while the peak velocity of the flow closer to the rear of the valve was 1.2 m/s. During the deceleration phase, the velocities of the forward jet and the flow along the trailing edge inside the valve decreased to 0.7 and 0.8 m/s respectively. RSS values ranging between 1,000 to 3,000 dyn/cm<sup>2</sup> were observed 35 mm downstream from the valve sewing ring at peak systole (Fig. 11). The corresponding RSS levels inside the valve along the trailing edge of the leaflet were approximately 800 dyn/cm<sup>2</sup>. The RSS levels inside the sinus region were close to zero throughout systole.

*Diastole*

The flow velocity downstream of the leaflet trailing edge during diastole was typically less than 0.01 m/s. No coherent vortex structure was observed in the sinus region and the velocities were typically less than 0.01 m/s. A leakage jet with a velocity of 0.3 m/s inside the valve near the commissural region of the top stent post persisted throughout diastole. The RSS levels throughout the measurement region were typically close to zero, except in the leakage jet inside the valve, where levels of approximately 300 dyn/cm<sup>2</sup> were seen.

*Prototype B Center Plane**Systole*

The flow characteristics observed in prototype B during the acceleration phase were similar to those in prototype A. At peak systole, the central orifice jet reached a maximum velocity of 2.1 m/s (Fig. 12). The central jet had a diameter of about 16 mm at the trailing edge of the leaflet. Prototype B displayed the same three lobe flow profile that was observed with prototype A; however, prototype B had a slightly slower forward flow jet (2.1 m/s) than prototype A (2.4 m/s). During systole the velocity in the sinus region was generally less than 0.07 m/s and no significant vortex structures were observed. The flow patterns inside proto-

type B during systole were similar to those observed in prototype A. Elevated velocities of approximately 2.0 m/s were typically observed along the leaflet trailing edge at peak systole, while the velocity along the stent inflow region was 0.5 m/s.

The RSS distribution observed in prototype B at peak systole was similar to that observed in prototype A. RSS values ranging between 500 and 3,000 dyn/cm<sup>2</sup> were observed along the edge of the central orifice jet and at the commissural region during systole.

*Diastole*

Figure 13 shows the center plane flow field downstream of prototype B during mid-diastole. The flow velocities downstream of the leaflet trailing edge were typically less than 0.04 m/s and the flow features during diastole were similar to those observed in prototype A. A leakage jet of 2.0 m/s was observed at the coaptation region inside the valve during valve closure. The jet persisted throughout diastole with velocities fluctuating between 0.6 and 2.0 m/s. A leakage jet of 0.73 m/s, not seen in prototype A, was intermittently observed at the commissural region of prototype B valve. During diastole, RSS values of approximately 5,000 dyn/cm<sup>2</sup> were occurred in the proximity of the leakage jet at the coaptation region as well as at the commissural region inside the valve.

*Prototype B + 8 mm Offset Plane**Systole*

During the acceleration phase, a forward flow jet of approximately 1.5 m/s emanated from the valve orifice near the commissural region (Fig. 14). Flow separation occurred at the leaflet trailing edge, with the reattachment points occurring beyond the measurement plane. A region of reverse flow, with a maximum velocity magnitude of 0.6 m/s, was evident at the lower edge of the central orifice jet corresponding to the formation of two vortices: one between the central forward jet and the reverse flow and another below the reverse flow. The flow patterns during the deceleration phase were similar to those observed at peak systole; however, both the central forward jet and the reverse flow reached a velocity of approximately 1.0 m/s. At peak systole, a forward flow with a maximum velocity of 1.6 m/s was recorded inside the valve at the leaflet trailing edge. Elevated RSS values between 600 and 3,000 dyn/cm<sup>2</sup> were confined mainly to the edge of the central orifice jet and the region between the reverse flow and the central jet. The RSS values inside the sinus region were less than 50 dyn/cm<sup>2</sup>.

*Diastole*

At mid-diastole, the flow inside the valve was dominated by a leakage jet near the commissural region



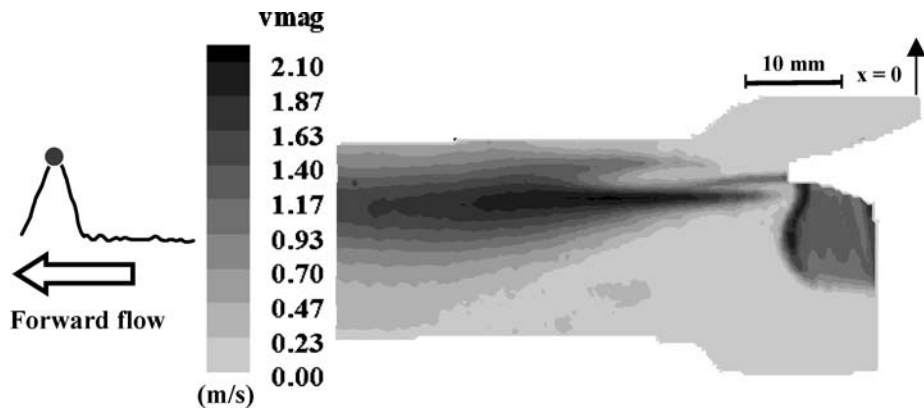


FIGURE 10. Velocity fields at the +8 mm offset plane of prototype A at peak systole. The central orifice jet reached the velocity of 2.1 m/s at peak systole. Elevated velocity of 2.0 m/s was also observed inside the valve near the trailing edge of the leaflet.

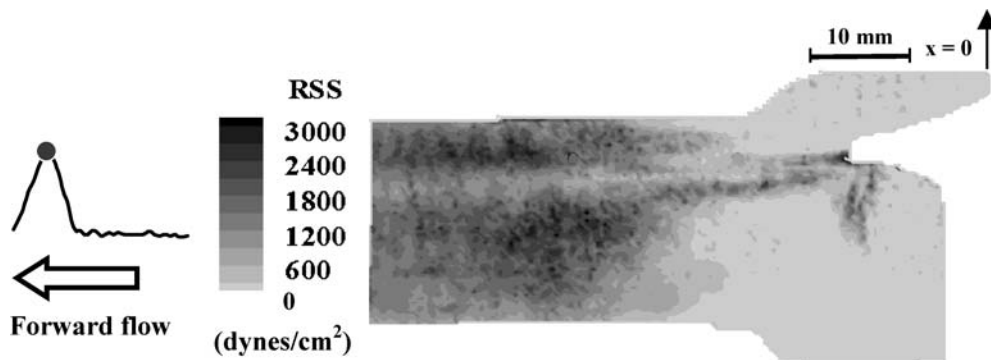


FIGURE 11. Reynolds shear stress (RSS) contour plot of the +8 mm offset plane of prototype A at peak systole. High RSS values coincided with regions of high velocity gradient typically observed at the edge of the central orifice jet.

with a velocity of approximately 0.6 m/s. This leakage jet persisted throughout diastole. A vortex occurred intermittently near the rear of the valve. A maximum RSS

of 2,000 dyn/cm<sup>2</sup> was recorded inside the valve in the leakage jet, while the RSS levels downstream of the leaflet and in the sinus region were typically less than 30 dyn/cm<sup>2</sup>.

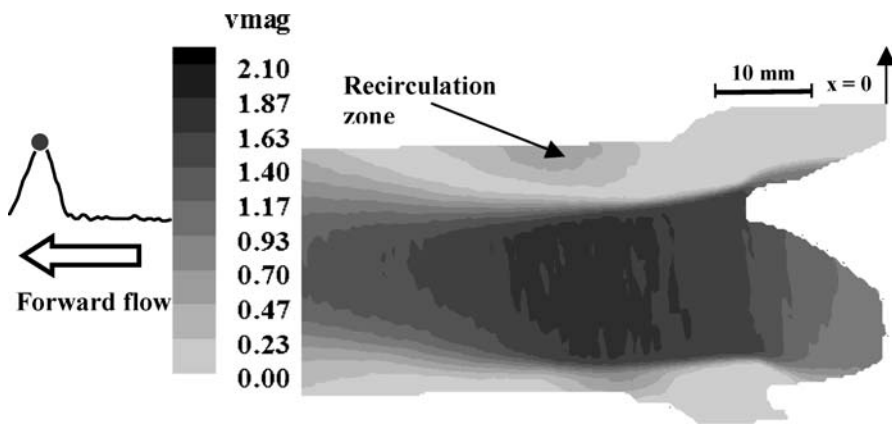


FIGURE 12. Phase-averaged velocity measurement at the center plane of prototype B at peak systole. Recirculation flow observed at the upper region of the flow chamber.

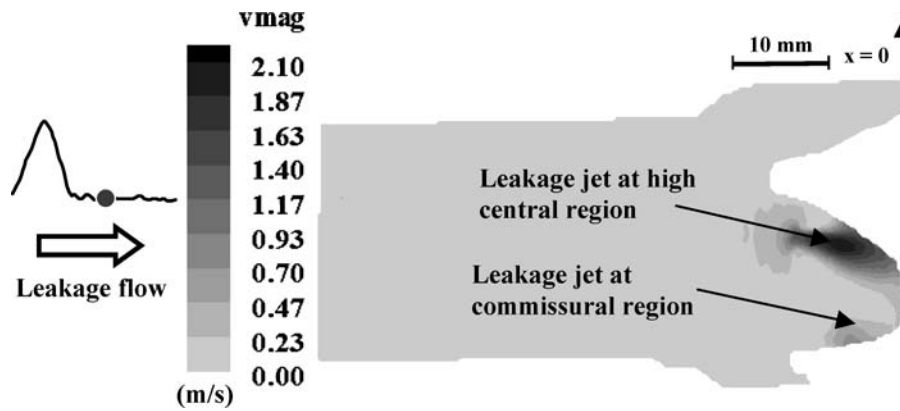


FIGURE 13. Phase-averaged velocity measurement at the center plane of prototype B during mid-diastole. Leakage jets were observed at both the high central and commissural regions inside the valve.

#### Prototype C Center Plane

##### Systole

During the acceleration phase, the flow characteristics were similar to those seen in prototype B. At peak systole (Fig. 15) the central orifice jet reached a maximum velocity of 2.1 m/s and a diameter of approximately 16 mm at the trailing edge of the leaflet. The central orifice jet had a flat profile when exiting the valve orifice but had become parabolic at a point approximately 50 mm downstream of the valve sewing ring. The velocity iso-surface of the central orifice jet of prototype C did not display the distinct three lobe feature seen in prototypes A and B; the flow profile became circular in shape as it approached the distal part of the flow chamber (55 mm downstream of the valve sewing ring). Velocities inside the sinus region were generally less than 0.04 m/s during systole and coherent vortex structures were not observed. The flow inside prototype C was similar to that observed in prototypes

A and B at peak systole. A maximum flow velocity of 1.8 m/s was reached inside the valve along the trailing edge of the leaflet, and a region of lower flow (0.78 m/s) was observed along the stent inflow region inside the valve. The flow velocity at the rear valve was approximately 1.4 m/s.

At peak systole RSS values of approximately 2,000 dyn/cm<sup>2</sup> were observed along the edge of the central orifice and at the commissural region of the valve. In contrast, the RSS in the central orifice jet and sinus regions were typically less than 45 dyn/cm<sup>2</sup>.

##### Diastole

Figure 16 shows the center plane flow field downstream of prototype C during mid-diastole. Flow patterns inside the valve during diastole were similar to those seen in prototype B. Two leakage jets were observed inside the valve during diastole: one in the coaptation region and one near the

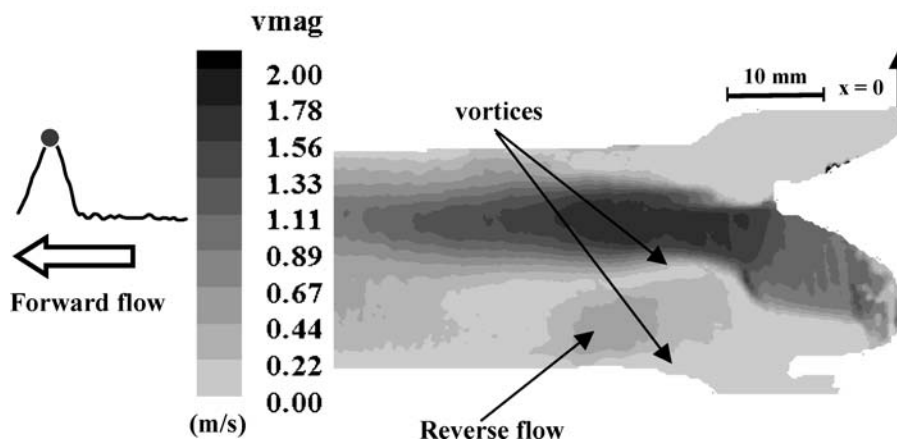
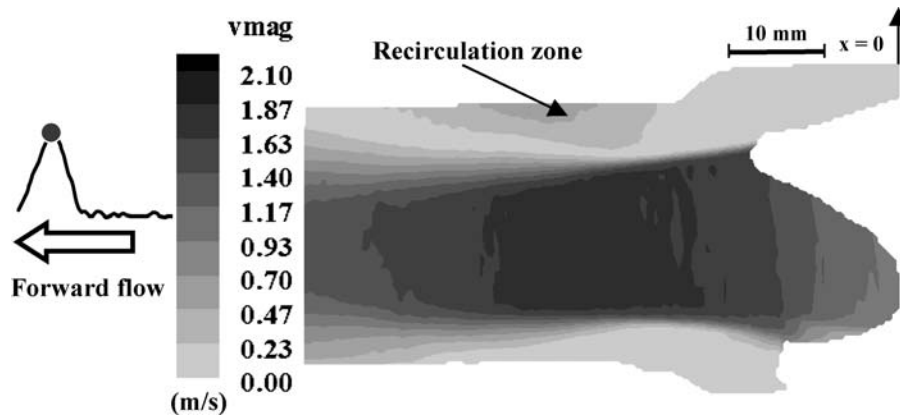


FIGURE 14. Phase-averaged velocity measurement at the + 8 mm offset plane of prototype B at peak systole. A region of reverse flow of magnitude 0.6 m/s was evident at the lower edge of the central orifice jet.



**FIGURE 15.** Phase-averaged velocity measurement at the center plane of prototype C at peak systole. A maximum velocity of 2.1 m/s was recorded inside the central orifice jet during peak systole.

commissural region of the valve. In addition to these leakage jets, a leakage flow of 0.57 m/s was seen occasionally along the trailing edge of the leaflet. The RSS levels downstream from the leaflet trailing edge during diastole were less than 50 dyn/cm<sup>2</sup>. Conversely, a peak RSS of 4,000 dyn/cm<sup>2</sup> was measured in the leakage jets inside the valve during diastole.

*Prototype C + 8 mm Offset Plane*

*Systole*

The flow characteristics observed in prototype C during the accelerating phase were similar to those in prototype A. During the acceleration phase, a forward flow jet of approximately 1.2 m/s emanated from the valve orifice with a vortex ring forming along the edge of the forward flow jet, approximately 25 mm downstream from the valve sewing ring. At peak systole, the flow inside the flow jet accelerated to 2.0 m/s (Fig. 17). The flow pattern inside prototype C was similar to that observed in prototypes A and B with a maximum velocity of approximately 1.7 m/s occurring

along the leaflet trailing edge. The flow patterns during the deceleration phase were similar to those observed at peak systole; however, both the central orifice jet and the flow along the leaflet trailing edge inside the valve had lower velocities, with a maximum of 0.7 m/s. At peak systole, RSS levels of approximately 3,000 dyn/cm<sup>2</sup> were recorded in the central region downstream of the valve at a point approximately 35 mm downstream of the sewing ring, corresponding to high velocity gradients at the edge of the central jet.

*Diastole*

During mid-diastole, the flow velocity throughout the entire measurement region was less than 0.1m/s with the exception of a leakage jet near the top stent post, which reached a maximum velocity of 0.26 m/s at mid-diastole and persisted throughout diastole. A maximum RSS of 2,250 dyn/cm<sup>2</sup>, coinciding with the location of this leakage jet, was recorded at the top stent post during diastole.

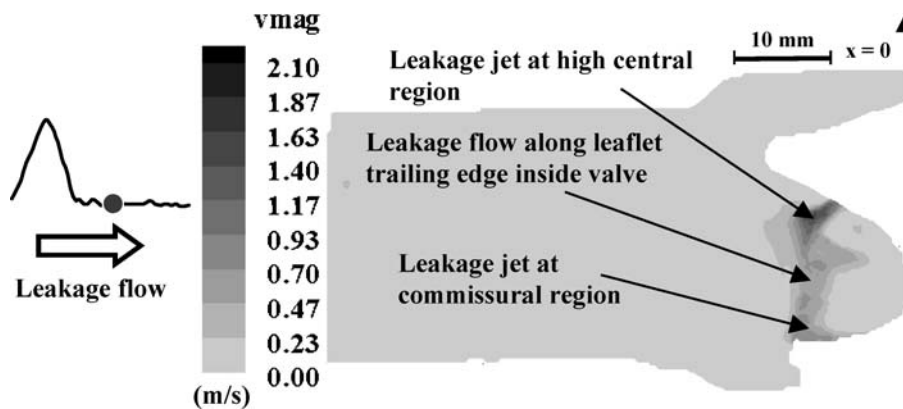


**FIGURE 16.** Phase-averaged velocity measurement at the center plane of prototype C during mid-diastole. Leakage jets of more than 0.7 m/s were seen at both the coaptation and the commissural region in the valve.

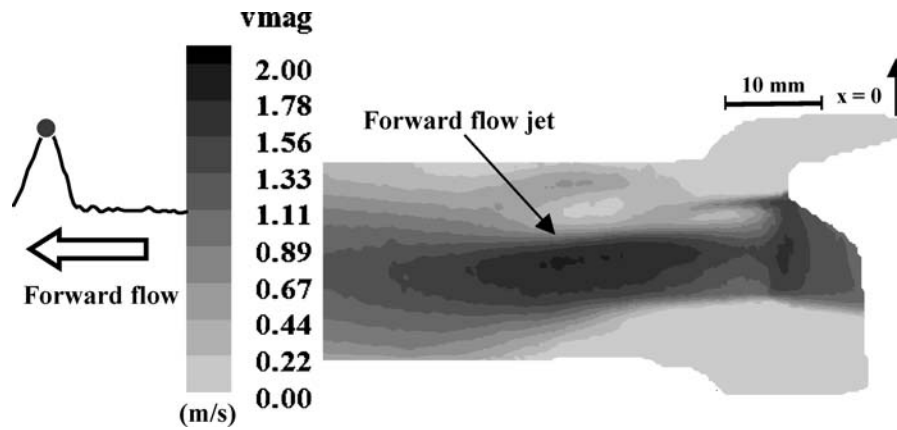


**FIGURE 17.** Phase averaged velocity measurement at the +8 mm offset plane of prototype C at peak systole. A maximum velocity of 2.0 m/s was recorded inside the forward flow jet at peak systole.

**DISCUSSION**

The results of this study are discussed in the following sequence: (1) the common flow structures of the three polymeric valves; (2) the differences in the flow fields observed in the valves; and (3) the influence of valve design on thrombus formation potential.

*Flow Field Characteristics Observed in All Three Polymeric Heart Valves*

*Flow Features Downstream of the Valves*

The velocity profile downstream of the leaflet trailing edge during systole was characterized by a central orifice jet, approximately 15 mm in diameter at the trailing edge of the leaflets and with peak forward velocities greater than 2.0 m/s during peak systole (Tables 1–3). The central orifice jet displayed a flat velocity profile immediately downstream of the leaflet trailing edge and developed a more parabolic profile 45 to 50 mm downstream from the valve sewing ring.

A vortex ring, with corresponding velocities of approximately 0.6 m/s, was observed as boundary layer instability along the leaflet trailing edge of the central orifice jet during the acceleration phase. As the leaflets opened, a crest was

formed on the leaflet surface producing a sudden increase in the flow area inside the valve and a corresponding contraction of the flow area at the edge of the leaflets. The change in leaflet shape caused a redirection and perturbation of the flow inside the valve, thus giving rise to the vortex ring during the acceleration phase.

Flow separation occurred at the leaflet trailing edge as the central orifice jet emerged from the valve orifice into the sinus region. In the center plane of all three valves, the central jet reattached approximately 50 mm downstream of the sewing ring in the lower part of the valve chamber, while in the upper part of the chamber reattachment of the flow occurred beyond the measurement plane. The difference in reattachment points between the upper and lower parts of the valve chamber is consistent with the asymmetrical nature of the central jet and the relative orientation of the measurement planes to the valve geometry. Low velocity flow (0.02 – 0.07 m/s) occurred inside the sinus region throughout systole, and a recirculation region was observed in the upper part of the flow chamber during systole.

Throughout diastole reverse flow with velocities between 0.2 and 0.4 m/s was observed along the leaflet trailing edge, and the location of this flow coincided with the valve coaptation region. A vortex, rotating in a clockwise

**TABLE 1.** Peak phased averaged velocity magnitudes (m/s) and corresponding RSS values (dyn/cm<sup>2</sup>) inside and downstream of prototype A during peak systole and diastole. The distance (mm) between the location where the peak values were recorded and the valve sewing ring are given in parenthesis.

| Measurement planes (mm) | Velocities (m/s) |          | RSS (dyn/cm <sup>2</sup> ) |           |
|-------------------------|------------------|----------|----------------------------|-----------|
|                         | Peak systole     | Diastole | Peak systole               | Diastole  |
| Center                  | 2.4 (20)         | 1.6 (7)  | 3,370 (40)                 | 9,000 (7) |
| ±4                      | 2.4 (22)         | 0.3 (15) | 4,190 (45)                 | 640 (15)  |
| ±8                      | 2.1 (25)         | 0.3 (15) | 3,110 (45)                 | 200 (15)  |
| ±12                     | 1.0 (40)         | <0.1     | 2,800 (42)                 | 45        |

**TABLE 2. Peak phased averaged velocity magnitudes (m/s) and corresponding RSS values (dyn/cm<sup>2</sup>) inside and downstream of prototype B during peak systole and diastole. The distance (mm) between the location where the peak values were recorded and the valve sewing ring are given in parenthesis.**

| Measurement planes (mm) | Velocities (m/s) |          | RSS (dyn/cm <sup>2</sup> ) |            |
|-------------------------|------------------|----------|----------------------------|------------|
|                         | Peak systole     | Diastole | Peak systole               | Diastole   |
| Center                  | 2.1 (25)         | 2.0 (6)  | 5,180 (45)                 | 12,650 (6) |
| ± 4                     | 2.1 (21)         | 0.5 (15) | 3,150 (40)                 | 2,300 (15) |
| ± 8                     | 2.0 (25)         | 0.3 (15) | 3,610 (40)                 | 1,590 (15) |
| ± 12                    | 1.0 (45)         | <0.1     | 2,180 (45)                 | 34         |

direction inside the sinus region, also persisted throughout diastole.

#### *Flow Features Inside the Valves*

The flow fields inside the three polymeric valves were similar throughout systole. Peak velocities greater than 2.0 m/s were observed along the leaflet trailing edge at peak systole. Flow velocities along the stent inflow region reached 0.5 m/s during the acceleration phase and reduced to less than 0.1 m/s in late systole. Complex flow structures were observed inside the valves during diastole and were characterized by leakage jets in the coaptation region with the velocity magnitude ranging from 0.5 to 2.0 m/s. Reverse flows were also observed along the leaflet trailing edge and intermittently at the commissural region. The flow inside the three prototype valves during diastole was characterized by a flow 'splitting' phenomenon where a portion of the flow was directed towards the center of the valve, i.e. towards the leakage jet at the high central region, while the remainder of the flow goes towards the stent inflow region. Previous studies with prototypes A and B using two component Laser Doppler Velocimetry (LDV) also showed the flow splitting characteristic, which was attributed to the combined influence of the closing dynamics of the valve and the persistent oscillation of the valve during diastole.<sup>16</sup> The persistence of the observed oscillation was believed to be due to the combined effect of both the leaflet thickness

and the flexibility of the valve frame.<sup>16</sup> LDV measurements near the frames of the three polymeric valves showed that the stent posts oscillate at a frequency of approximately 12–14 Hz during diastole.<sup>16</sup>

#### *Differences in the Flow Fields*

##### *Flow Features Downstream of the Valves*

Compared to the other two valves, prototype A displayed slightly higher velocities downstream of the valve, which is consistent with the smaller effective flow orifice resulting from its closed commissural design (Tables 1–3). Reconstructions of the 3D velocity fields at peak systole show that the central orifice jet in the three polymeric heart valves has a three-lobe flow configuration. Each lobe on the velocity iso-surface (Fig. 7) represents a high velocity flow emanating from the commissural region. The three-lobe flow feature was most evident 50 mm downstream from the valve sewing ring and was much more distinct in prototype A than in prototypes B and C. This is due to the closed commissural design of prototype A, which resulted in a smaller effective flow area compared to prototypes B and C. This observation also explains the fact that a higher central orifice jet velocity was recorded in prototype A than in prototypes B and C. Accordingly, prototype A produced a smaller central orifice jet with a diameter of 13 mm compared with the 16 mm diameter central orifice jet seen in prototypes B and C.

**TABLE 3. Peak phased averaged velocity magnitudes (m/s) and corresponding RSS values (dyn/cm<sup>2</sup>) inside and downstream of prototype A during peak systole and diastole. The distance (mm) between the location where the peak values were recorded and the valve sewing ring are given in parenthesis.**

| Measurement planes (mm) | Velocities (m/s) |           | RSS (dyn/cm <sup>2</sup> ) |            |
|-------------------------|------------------|-----------|----------------------------|------------|
|                         | Peak systole     | Diastole  | Peak systole               | Diastole   |
| Center                  | 2.1 (25)         | 0.73 (15) | 2,500 (40)                 | 4,500 (15) |
| ± 4                     | 2.1 (26)         | 0.8 (15)  | 3,280 (42)                 | 2,080 (15) |
| ± 8                     | 2.6 (23)         | 0.3 (15)  | 3,780 (40)                 | 150 (15)   |
| ± 12                    | 0.8 (45)         | < 0.4     | 1,870 (4)                  | 55         |



Comparison of the velocity distribution between the offset planes showed that the flows were generally symmetrical, especially during peak systole, but less so during the diastolic phase. The closing dynamics of the valve leaflet and the oscillation of the valve during diastole may give rise to the observed flow asymmetry in these offset measurement planes.

In prototype B the jet appeared to reattach to the upper part of the flow chamber 50 mm downstream from the valve sewing ring while in prototypes A and C this flow reattachment occurred at a location beyond the measurement plane. An explanation for this observation is that the open commissural design of prototype B caused the central orifice jet to be directed more towards the upper part of the flow chamber and earlier reattachment.

#### *Flow Features Inside the Valves*

Leakage jets were observed in the high central region of all three valves. A comparison of prototypes A and B shows that the velocities and RSS levels of the leakage jet in prototype B (2.0 m/s; 12,650 dyn/cm<sup>2</sup>) were higher and larger than in prototype A (1.6 m/s; 9,000 dyn/cm<sup>2</sup>) (Tables 1 and 2). This may be due to the thicker, and therefore less compliant leaflets of prototype B, which may not close completely during diastole. Comparing all three valves, the leakage jet at the high central region of prototypes A and B were relatively more well-defined than in prototype C where the leakage jet appeared only intermittently throughout diastole, and tended to mix with the retrograde flow along the leaflet trailing edge. An additional leakage jet, not seen in prototype A, was observed at the commissural region of prototypes B and C and is attributed to their respective open and semi-open commissural designs. It appears that the leaflets at the commissural region of prototypes B and C generated a large gap channel at the stent during diastole, thereby permitting leakage flow to occur along the stent inflow region.

#### *Influence of Valve Design on Thrombus Formation Potential*

Animal studies using sheep have shown that polymeric valves are prone to material degradation as a result of extrinsic calcification of the attached host biological material on the leaflet surface.<sup>6,7,22</sup> These studies found local fibrin deposits in the commissural regions and attributed these deposits to inefficient washout. Preliminary *in vivo* experiments involving prototypes A and B also showed thrombus formation along the commissure in the stent inflow region of both designs and in the high central region of prototype B. Thrombus deposit along the stent inflow region of prototype A was initially believed to be caused by an inefficient washout of the closed commissural region.<sup>16</sup>

However, subsequent animal experiments with prototype B (open commissural design) showed similar thrombus formation along the stent region, indicating that commissural design is not the sole contributor to thrombus formation. The present fluid dynamic study suggests that the observed clots in prototypes A and B are due to two main factors: the elevated RSS levels in the vicinity of the prototype valves, and the flow structures observed inside the valve during diastole. The high fluid shear stress occurring during systole may lead to blood elements damage and activation, while the low velocity fluid structures such as the split flow inside the valves during diastole may enhance the interaction of the damaged blood elements and contribute to subsequent thrombi buildup in the valve superstructure. Currently, there are no animal results available for prototype C.

Recent research involving various mechanical and tissue heart valves has shown the importance of RSS calculation as a means of quantifying the damage of blood elements in valve prostheses. Previous studies reported that hemolysis can occur for RSS threshold values ranging from as low as 400 dyn/cm<sup>2</sup> to 5,600 dyn/cm<sup>2</sup> with exposure time ranging from 10<sup>2</sup> to 10<sup>-4</sup>s. For platelet activation, the reported RSS threshold ranges between 100 and 1,000 dyn/cm<sup>2</sup> with exposure time varying from 10<sup>2</sup> to 10<sup>-2</sup>s.<sup>8,9,17</sup>

The results from the present polymeric valve experiments enable identification of several regions of high shear stress where the potential for platelet activation, hemolysis, and subsequent thrombus formation is high. During peak systole, elevated RSS values of more than 3,000 dyn/cm<sup>2</sup> were observed along the edge of the central orifice jet, along the leaflet trailing edge, and at the distal region of the valve chamber 40 mm downstream from the sewing ring where the central orifice jet mixed with the surrounding fluid. During diastole, high RSS levels exceeding 4,000 dyn/cm<sup>2</sup> were observed in the leakage jets inside the valve. In the regions of elevated RSS, the exposure time of the fluid to the high Reynolds shear stress was between 120 and 300 ms. The level and duration of these RSS values, ranging from 2,000 dyn/cm<sup>2</sup> to more than 13,000 dyn/cm<sup>2</sup>, are above the threshold values reported in the literature for red blood cell damage and platelet activation.<sup>8, 9, 17</sup>

Regions of low flow velocities that would promote the interaction of activated blood elements were observed in the following regions of the three polymeric heart valves during diastole: (1) the split flow inside the valve; (2) the vortex inside the sinus region; and (3) the flow inside the recirculation zone along the chamber wall. This flow 'splitting' phenomenon may also enhance the transportation of activated blood elements towards the stent inflow and high central regions of the valve during diastole. In both prototypes B and C, the strength of the split flow increased when the intermittent leakage jets were present at the high central and the commissural regions. Therefore, it is likely

**TABLE 4. Comparison of the velocity magnitudes and Reynolds shear stresses from various trileaflet valve designs**

|  | Effective annular orifice diameter (mm) | Maximum phase averaged velocity during systole (m/s) | Maximum phase averaged RSS during systole (dyn/cm <sup>2</sup> ) |
|--|---|--|--|
| Carpentier-Edwards 2625 porcine valve (27 mm)        | 23.0                                    | 3.3  | 4,500  |
| Hancock modified orifice porcine valve (25 mm)       | 21.8                                    | 3.0  | 2,900  |
| Ionescu-Shiley pericardial valve (27 mm)             | 23.4                                    | 2.3  | 2,500  |
| Carpentier-Edwards 2650 porcine valve (27 mm)        | 25.0                                    | 2.0  | 2,000  |
| Hancock II porcine valve (27 mm)                     | 24.0                                    | 2.6  | 2,500  |
| Hancock pericardial valve (27 mm)                    | 23.3                                    | 1.8  | 2,100  |
| Ionescu-Shiley low profile pericardial valve (27 mm) | 23.0                                    | 2.2  | 2,400  |
| Carpentier-Edwards pericardial valve (27 mm)         | 25.7                                    | 1.8  | 1,000  |
| Abiomed (21 mm)                                      | 18.6                                    | 3.7  | 4,500  |
| Abiomed (25 mm)                                      | 22.8                                    | 2.2  | 2,200  |
| Aortech prototype A (23 mm)                          | 23.0                                    | 2.8  | 4,190  |
| Aortech prototype B (23 mm)                          | 23.0                                    | 2.5  | 5,180  |
| Aortech prototype C (23 mm)                          | 23.0                                    | 2.3  | 3,780  |

that these leakage jets contribute to the formation of split flow.

A preliminary animal study also revealed thrombus formation in the high central region of prototype B along the leaflet machining lines (from personal communications with Aortech Inc.). These machining lines, not evident on prototype A, were created during the fabrication process in which the polyurethane frames of the leaflet are mounted onto steel formers leaving indentations on the inflow side of the leaflets.<sup>18</sup> It is likely that the combined influence of these machining lines and the elevated shear stresses reported in this study in the leakage jet of prototype B were responsible for the observed clot buildups.

#### *Comparison of Current Aortic Polymeric Valves Studies with Previous Experiments*

Important studies investigating the *in vitro* hemodynamic characteristics of tissue and polymeric heart valves performed in the past two decades have revealed complex flow structures in the vicinity of the trileaflet valve prostheses, corroborating the findings of the current experiments with the three polymeric heart valves.<sup>23–26</sup> The diameter of the central jets in the tissue bioprostheses at peak systole is typically larger than that in the polymeric heart valves. The bioprosthetic valves have larger tissue annular diameters compared with the polymeric prostheses (see Table 4). For a given cardiac output, valves with larger tissue annular diameters typically have larger jet diameter compared to those with smaller tissue annular diameters. Central orifice jet diameters between 15 and 25 mm were observed in the bioprostheses at peak systole with the smallest occurring in Carpentier-Edwards 2625 and Hancock standard-orifice porcine valves, and the largest in the Hancock pericardial and Carpentier-Edwards pericardial valves. The jet

diameters for the three Aortech polymeric heart valves were comparable to that of the Abiomed trileaflet polymeric valve prosthesis, which had a jet diameter of 14 mm.<sup>23, 24</sup> The Aortech prototype A had a jet diameter of 13 mm while both Aortech prototypes B and C had a jet diameter of 16 mm.

Table 4 compares the peak velocities and RSS values of previous valve studies with those obtained in the current polymeric valve experiments. The peak RSS levels calculated downstream of all valves during systole was typically between 1,000 and 4,500 dyn/cm<sup>2</sup>. The highest RSS of 5,180 dyn/cm<sup>2</sup> was recorded in Aortech prototype B, while both the Abiomed 21 mm and the Carpentier-Edwards 27 mm 2625 porcine valves recorded RSS of 4,500 dyn/cm<sup>2</sup>. Elevated RSS levels were typically observed along the edge of the central orifice jet and were spread out over a wider area farther downstream from the valve as the energy of the central jet dissipated. All of the aortic valves studied produced RSS in excess of 200 dyn/cm<sup>2</sup> during the majority portion of systole. It is therefore clear that the elevated RSS levels could lead to sub-lethal and/or lethal damage to blood elements.

## CONCLUSIONS

This study employed 3D PIV technique to investigate the flow fields inside three polymeric heart valves and assess the effect of valve design on the thrombus formation potential of the prosthesis. Design parameters, including the leaflet thickness and commissural design, clearly influence the flow structures inside and downstream of the valve. The valve with thicker leaflets (120  $\mu$ m) produced greater leakage flow during the diastolic phase compared to the thinner 80  $\mu$ m thickness leaflet valve. Additionally, the split flow patterns inside all valves were consistent with the blood clots observed along the inflow stent region of the

valve in the animal experiments,<sup>6,7</sup> suggesting that none of the commissural designs (open, closed or semi-open) were able to ensure sufficient washout inside the valve during systole. Reconstruction of the 3D PIV results reveals a three-lobe iso-surface of the flow profile downstream of the three valves. This profile can be attributed to the configuration of the open leaflets during systole and is the most distinct in the closed commissural design.

Several flow regions with high RSS levels and elevated velocities were identified: (1) the leakage jet inside the valve during diastole, (2) the flow along the leaflet trailing edge during the systole, (3) the edge of the central orifice jet, extending from the inside of the valve to approximately 50 mm downstream of the valve sewing ring, and (4) turbulent mixing occurring at the distal region of the flow chamber 40 mm downstream of the sewing ring during systole. These regions of high fluid stresses may contribute to the activation of blood elements.

Lower velocity flow structures, including a split flow feature, were observed inside the valve during diastole. The split flow phenomenon is attributed to the leakage jets and the oscillation of the valve leaflets during early diastole and may enhance the transportation of activated/lysed blood cells towards the stent region, leading to subsequent thrombus buildup in the valve superstructure.

In summary, the leaflet thickness was found to influence the size of the leakage jets inside the valve during diastole. Even though the commissural design may influence the flow and therefore the thrombus formation at the commissural region, a clear link between commissural design and clot formation along the stent inflow region has not been found. However, the high shear stress along the edge of the central orifice forward jet during systole and the split flow, observed inside all three valves during diastole, were identified as possible factors contributing to the blood clot formation observed along the stent in previous *in vivo* studies.

### EXPERIMENTAL LIMITATIONS

A major constraint to the current aortic valve studies was that only three different valve designs were investigated. Further work involving more valve designs would provide a much broader understanding of the effect of design parameters on the flow fields of polymeric valves. However, the author believes that the current studies set the ground work for further *in vitro* studies that focus on the hemodynamic aspects of polymeric heart valve design.

### ACKNOWLEDGMENTS

This work was partially supported by a grant from the National Heart, Lung and Blood Institute (HL 720621). The authors wish to thank Aortech, Inc for providing the prototype valves.

### REFERENCES

- <sup>1</sup>Bernacca, G. M., T. G. Mackay, M. J. Gulbransen, A. W. Donn, and D. J. Wheatley. Polyurethane heart valve durability: Effects of leaflet thickness and material. *Int. J. Artif. Organs* 20(6):327–331, 1997.
- <sup>2</sup>Bernacca, G. M., T. G. Mackay, R. Wilkinson, and D. J. Wheatley. Calcification and fatigue failure in a polyurethane heart valve. *Biomaterials* 16(4):279–285, 1995.
- <sup>3</sup>Bernacca, G. M., B. O'Connor, D. F. Williams, and D. J. Wheatley. Hydrodynamic function of polyurethane prosthetic heart valves: Influences of Young's modulus and leaflet thickness. *Biomaterials* 23(1):45–50, 2002.
- <sup>4</sup>Bodnar, E., and R. Frater, eds. Replacement Cardiac Valves. New York: Pergamon press, 1991, p.482.
- <sup>5</sup>Chandran, K. B., R. Fatemi, R. Schoepfoerster, D. Wurzel, G. Hansen, G. Pantalos, L. S. Yu, and W. J. Kolff. In vitro comparison of velocity profiles and turbulent shear distal to polyurethane trileaflet and pericardial prosthetic valves. *Artif. Organs* 13(2):148–154, 1989.
- <sup>6</sup>Daebritz, S. H., B. Fausten, B. Hermanns, J. Schroeder, J. Groetzner, R. Autschbach, B. J. Messmer, and J. S. Sachweh. Introduction of a flexible polymeric heart valve prosthesis with special design for aortic position. *Eur. J. Cardiothorac. Surg.* 25(6):946–952, 2004.
- <sup>7</sup>Daebritz, S. H., J. S. Sachweh, B. Hermanns, B. Fausten, A. Franke, J. Groetzner, B. Klosterhalfen, and B. J. Messmer. Introduction of a flexible polymeric heart valve prosthesis with special design for mitral position. *Circulation* 108 (Suppl 1):II134–II139, 2003.
- <sup>8</sup>Ellis, J. T., T. M. Healy, A. A. Fontaine, R. Saxena, and A. P. Yoganathan. Velocity measurements and flow patterns within the hinge region of a Medtronic Parallel bileaflet mechanical valve with clear housing. *J. Heart Valve Dis.* 5(6):591–599, 1996.
- <sup>9</sup>Ellis, J. T., and A. P. Yoganathan. A comparison of the hinge and near-hinge flow fields of the St Jude medical hemodynamic plus and regent bileaflet mechanical heart valves. *J. Thorac. Cardiovasc. Surg.* 119(1):83–93, 2000.
- <sup>10</sup>Goldsmith, I., S. Mukundan, A. Nugent, and M. D. Rosin. Early clinical experience with the Tissuemed porcine bioprosthesis. *Ann. Thorac. Surg.* 66(Suppl 6 ):S259–S263, 1998.
- <sup>11</sup>Herold, M., H. B. Lo, H. Reul, H. Muckter, K. Taguchi, M. Giesiepen, G. Birkle, G. Hollweg, G. Rau, and B. J. Messmer. The Helmholtz-institute-tri-leaflet-polyurethane-heart valve prosthesis: Design, manufacturing and first in-vitro and in vivo results. In: Polyurethanes in Biomedical Engineering II, edited by H. E. A. Planck. Elsevier Science Publishers, 1987, pp. 231–268.
- <sup>12</sup>Hyde, J. A., J. A. Chinn, and R. E. Phillips Jr.. Polymer heart valves. *J. Heart Valve Dis.* 8(3):331–339, 1999.
- <sup>13</sup>Jamieson, W. R., L. H. Burr, W. N. Anderson Jr., J. B. Chambers, J. P. Gams, and C. M. Dowd. Prosthesis-related complications: First-year annual rates. *J. Heart Valve Dis.* 11(6):758–763, 2002.
- <sup>14</sup>Jansen, J., S. Willeke, B. Reiners, P. Harbott, H. Reul, H. B. Lo, S. Dabritz, C. Rosenbaum, A. Bitter, and K. Ziehe. Advances in design principle and fluid dynamics of a flexible polymeric heart valve. *ASAIO Trans.* 37(3):M451–M453, 1991.
- <sup>15</sup>Leat, M. E., and J. Fisher. The influence of manufacturing methods on the function and performance of a synthetic leaflet heart valve. *Proc. Inst. Mech. Eng. [H]*. 209(1):65–69, 1995.
- <sup>16</sup>Leo, H. L., H. Simon, J. Carberry, S. C. Lee, and A. P. Yoganathan. A comparison of flow field structures of two

- tri-leaflet polymeric heart valves. *Ann. Biomed. Eng.* 33(4):429–443, 2005.
- <sup>17</sup>Lu, P. C., H. C. Lai, and J. S. Liu. A reevaluation and discussion on the threshold limit for hemolysis in a turbulent shear flow. *J. Biomech.* 34(10):1361–1364, 2001.
- <sup>18</sup>Mackay, T. G., D. J. Wheatley, G. M. Bernacca, A. C. Fisher, and C. S. Hindle. New polyurethane heart valve prosthesis: Design, manufacture and evaluation. *Biomaterials* 17(19):1857–1863, 1996.
- <sup>19</sup>Sallam, A. M., and N. H. Hwang. Human red blood cell hemolysis in a turbulent shear flow: Contribution of Reynolds shear stresses. *Biorheology* 21(6):783–797, 1984.
- <sup>20</sup>Turitto, V. T., and C. L. Hall. Mechanical factors affecting hemostasis and thrombosis. *Thromb. Res.* 92(6 Suppl 2):S25–S31, 1998.
- <sup>21</sup>Vyavahare, N., M. Ogle, F. J. Schoen, R. Zand, D. C. Gloeckner, M. Sacks, and R. J. Levy. Mechanisms of bioprosthetic heart valve failure: Fatigue causes collagen denaturation and glycosaminoglycan loss. *J. Biomed. Mater. Res.* 46(1):44–50, 1999.
- <sup>22</sup>Wheatley, D. J., G. M. Bernacca, M. M. Tolland, B. O'Connor, J. Fisher, and D. F. Williams. Hydrodynamic function of a biostable polyurethane flexible heart valve after six months in sheep. *Int. J. Artif. Organs.* 24(2):95–101, 2001.
- <sup>23</sup>Woo, Y. R., F. P. Williams, and A. P. Yoganathan. In-vitro fluid dynamic characteristics of the abiomed trileaflet heart valve prosthesis. *J. Biomech. Eng.* 105(4):338–345, 1983.
- <sup>24</sup>Woo, Y. R., F. P. Williams, and A. P. Yoganathan. Steady and pulsatile flow studies on a trileaflet heart valve prosthesis. *Scand. J. Thorac. Cardiovasc. Surg.* 17(3):227–236, 1983.
- <sup>25</sup>Yoganathan, A. P. Cardiac valve prostheses. In: *The Biomedical Engineering Handbook*. CRC Press LLC, pp. 127-1–127-23, 2000.
- <sup>26</sup>Yoganathan, A. P., Y. R. Woo, H. W. Sung, F. P. Williams, R. H. Franch, and M. Jones. In vitro hemodynamic characteristics of tissue bioprostheses in the aortic position. *J. Thorac. Cardiovasc. Surg.* 92(2):198–209, 1986.